Mixture of Azolium Tetraphenylborate with Isopropylthioxanthone: a New Class of N-Heterocyclic Carbene (NHC) Photogenerator for Polyurethane, Polyester and ROMP Polymers Synthesis

Thi Kim Hoang Trinh, Jean-Pierre Malval, Fabrice Morlet-Savary, Julien Pinaud, Patrick Lacroix-Desmazes, Corine Reibel, Valérie Héroguez, Abraham Chemtob

Mixture of Azolium Tetraphenylborate with Isopropylthioxanthone: a New Class of N-Heterocyclic Carbene (NHC) Photogenerator for Polyurethane, Polyester and ROMP Polymers Synthesis

Thi Kim Hoang Trinh,[a,b] Jean-Pierre Malval,[a,b] Fabrice Morlet-Savary,[a,b] Julien Pinaud,[c] Patrick Lacroix-Desmazes,[c] Corine Reibel,[c] Valérie Héroguez,[d] and Abraham Chemtob*[a,b]

[a] Institut de Science des Matériaux de Mulhouse, IS2M UMR 7361 CNRS, Université de Haute-Alsace, France
[b] Université de Strasbourg, France
[c] Institut Charles Gerhardt Montpellier, ICGM UMR 5253 Université de Montpellier, CNRS, ENSCM, Montpellier, France
[d] Université de Bordeaux, CNRS, Bordeaux INP, LCPO, UMR 5629, F-33600, Pessac, France

Abstract: In the search of smarter routes to control the conditions of N-heterocyclic carbenes (NHCs) formation, a two-component air-stable NHC photogenerating system is reported. It relies on the irradiation at 365 nm of a mixture of 2-isopropylthioxanthone (ITX) with 1,3-bis(mesityl)imidazoli(ni)um tetraphenylborate. The photoinduced liberation of NHC is evidenced by reaction with a mesitoyl radical to form a NHC-radical adduct detectable by electron spin resonance spectroscopy. The NHC yield can be determined by ^{1}H NMR through the formation of a soluble and stable NHC-carbodiimide adduct. To deprotonate the azolium salt and liberate the NHC, a mechanism is proposed where the role of base is played by ITX radical anion formed in situ by a primary photoinduced electron-transfer reaction between electronically excited ITX (oxidant) and BPh_4^- (reductant). A NHC yield as high as 70 % is achieved upon starting with a stoichiometric ratio of ITX and azolium salt. Three different photoNHC-mediated polymerizations are described: synthesis of polyurethane and polyester by organocatalyzed step-growth polymerization and ring-opening copolymerization, respectively, and generation of polynorbornene by ring-opening metathesis polymerization using a NHC-coordinated Ru catalyst formed in situ.

Introduction

In a ground-breaking work, Arduengo et al. presented in 1991 the first successful isolation of a stable *N*-heterocylic carbene (NHC).[1] Since this achievement, NHCs have been at the forefront of organometallic chemistry,[2,3] catalysis,[4] and more recently polymerization.[5] To date, the most frequently encountered NHCs are 1,3-bis(mesityl)imidazol-2-ylidene (IMes, **1**) and its saturated congener 1,3-bis(mesityl)imidazolidin-2-ylidene (SIMes, **2**) (**Figure 1**). Thanks to their excellent σ-donor ability, the NHC ligands have gradually replaced phosphines, that are not environmentally benign.[6–8] After reaction with transition metals, they can form well-defined NHC-metal complexes displaying outstanding catalytic activity. The most prominent examples are the ruthenium alkylidene complexes coordinated with NHC ligand used in olefin metathesis, including the so-called Hoveyda–Grubbs second-generation catalyst and

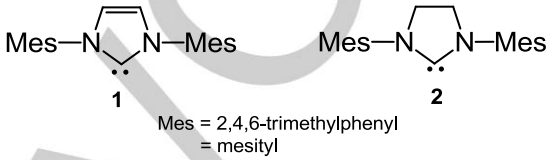

Figure 1. 1 and **2** are among the most frequently employed NHCs.

its multiple derivatives.[9] In addition, their strong nucleophilicity and Brønsted basicity have contributed to their use as organocatalysts. In polymerization, they can replace organometallic compounds with advantages of reducing cost and toxicity. The range of NHC-mediated polymerizations[5,10,11] already covers ring-opening polymerization (lactone,[12] lactam,[13] epoxide[14]) as well as step-growth polymerization for the synthesis of polybenzoin[15] or polyurethane.[16]

Despite the wealth of research conducted to date, the practical use of NHCs presents a number of challenges: NHCs are highly sensitive to moisture, and must be handled under dry atmosphere. Moreover, they react with acids due to their high pK_a, and are also prone to dimerization.[17,18] Because of these constraints, NHCs are usually put in contact with substrates or monomers at the last moment. Considering the central role of NHCs in chemistry, it is essential to control and optimize their formation conditions. The issues are to facilitate storage, handling, processing, and more broadly, to promote scale-up from laboratory to production. Currently, *in situ* deprotonation of an azolium salt is by far the most commonly used methodology to access a free or ligated NHC.[19–21] However, this methodology requires a strong base, that limits the scope of substrates and may interfere in the polymerization process as adventitious initiator.[22] In the search of smarter routes for *in situ* and "on demand" release of NHC, "masked" or "protected" NHCs have been investigated recently.[22,23] Of high interest are thermally-labile NHC progenitors based on air-stable NHC-CO_2 adduct,[24] NHC-isothiocyanate adduct[25] or NHC-metal complex.[26] Upon heating, the adduct/complex bond may be broken and the carbene transferred. Despite promising results, such approach has important limitations related to reversible cleavage, poor solubility of many NHC adducts, incomplete latency at ambient conditions resulting in early reaction, byproducts' formation, and additional energy expense due to heating.[22]

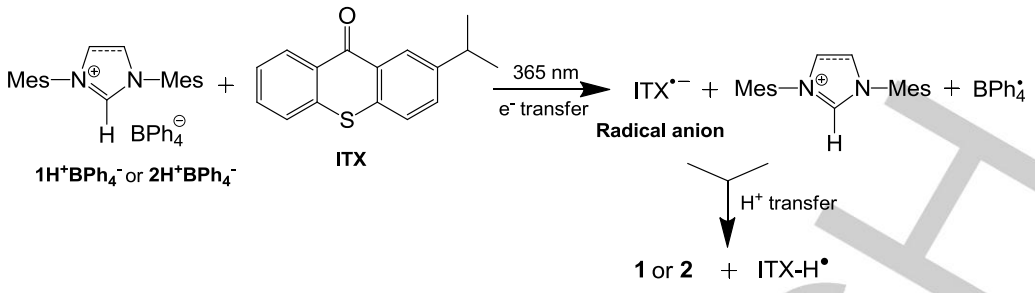

Scheme 1. Photolysis mechanism for the photogeneration of **1** (or **2**) from the bicomponent photogenerating system ITX/**1H$^+$BPh$_4^-$** (or ITX/**2H$^+$BPh$_4^-$**).

Despite the many developments in the field of photoinitiators,[27,28] very little attention has been given to photolatent NHC precursors. In 2015, Denning et al.[29] reported the photochemical reduction of an imidazolium-2-carboxylate (NHC-CO_2) using an excited state electron donor, N,N,N′,N′-tetramethylbenzidine. The reduced formate complex might then decompose into NHC and formate ion. However, the authors only detected the corresponding imidazolium (the conjugated acid of the NHC), which was not an issue because the principal goal was actually the controlled capture and release of CO_2. The limited research effort on NHC photogenerator is in contrast with the strong interest for other photobase generators (PBGs), capable of releasing amidine or guanidine organosuperbases.[30] Most PBGs proceed through a photoinduced proton transfer reaction employing a salt containing the protonated superbase and an anion chromophore based on ketoprofene,[31] thioxanthone derivatives,[32] and tetraphenylborate.[33–35]

Today, there are strong motivations for developing photoNHC-mediated reactions: temporal and spatial control of reaction, use of a contactless stimulation, and NHC release at ambient condition by precise energetic and spatial dosage of radiation. Our aim is to design a novel NHC photogenerator, both stable in absence of light and capable of releasing *in situ* free NHC under UV exposure, preferentially UVA (320 – 400 nm) to avoid substrate or solvent excitation. For this purpose, imidazolium or imidazolinium salts seem the most appropriate photolatent NHC precursors. Like many ionic liquids, they are air/moisture stable, thermally inert and chemically quite stable. The challenge is thus how to promote a photochemically induced proton transfer reaction that would convert the starting inactive azolium salt into an active NHC. The proposed solution is to produce a suitable radical anion via a photoinduced electron-transfer (PET) reaction, which can subsequently deprotonate the azolium cation (**Scheme 1**). To this end, we begin with a mixture of isopropylthioxanthone (ITX) with an air-stable azolium tetraphenylborate salt, such as 1,3-bis(mesityl)imidazolium tetraphenylborate **1H$^+$BPh$_4^-$** or 1,3-bis(mesityl)imidazolinium tetraphenylborate **2H$^+$BPh$_4^-$**.[36] First, ITX is an inexpensive, commercially available aryl ketone, known for its ability to mediate single electron-transfer after photochemical excitation in the near UV-Vis region (350 - 420 nm); in particular, excited ITX is used as an electron acceptor sensitizer in many photoreactions.[37] On the other hand, the tetraphenylborate anion may act as suitable electron donating partner to make PET thermodynamically feasible.[38,39] Therefore, the expected primary photochemical process is electron-transfer from BPh_4^- to triplet ITX. In second step, the resulting intermediate ITX radical anion might effectively abstract proton from **1H$^+$** (or **2H$^+$**) to form NHC **1** (or **2**).

Encouraged by preliminary results proving the release of NHC upon irradiation,[36] this current work describes a comprehensive study of this new class of bicomponent NHC photogenerator — ITX/**1H$^+$BPh$_4^-$** and ITX/**2H$^+$BPh$_4^-$** — with four distinct parts. Firstly, we propose two novel analytical methods to characterize the photochemically released NHCs through their conversion in suitable adducts: carbene-radical adduct enables an identification method by using electron spin resonance (ESR) spectroscopy, while stable NHC-carbodiimide adduct facilitates the quantification of photoNHC yield using ^{1}H NMR. Secondly, to support the 2-step photochemical pathway based on electron/proton transfer reactions, experiments of real-time photobleaching of ITX are performed as well as calculation of the free energy change of electron-transfer with Rehm-Weller equation. Thirdly, using a mechanism-guided approach, NHC yield are optimized by investigating the effect of irradiation time, sensitizer concentration and structure. In a last part, the NHC photogenerator is harnessed to prepare a variety of polymer structures through their twofold role. As organocatalyst, polyurethane and polyester were prepared by step-growth polymerization and ring-opening copolymerization, respectively. As ligand, polynorbornene was synthesized by ring-opening metathesis polymerization (ROMP) using a NHC-coordinated Ru catalyst.

Results and Discussion

1. Identification and quantification of photogenerated NHC

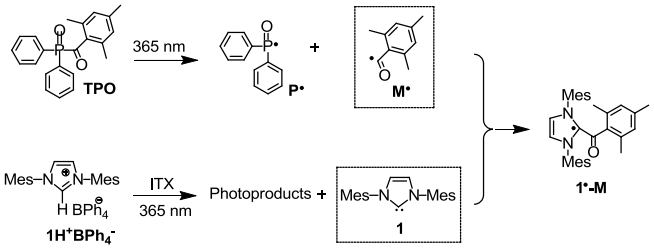

Scheme 2. Reaction pathway to generate NHC-radical adduct after irradiation of ITX/**1H$^+$BPh$_4^-$** in presence of TPO.

ESR spectroscopy of NHC-radical adduct: Identification of NHC. **1H$^+$BPh$_4^-$** or **2H$^+$BPh$_4^-$** (3 equiv.) were mixed with ITX (1 equiv.) under ambient conditions in THF-d_8. In the absence of light, the mixture is stable supporting that in its ground state, ITX cannot participate in an electron-transfer reaction. In either case, the ^{1}H NMR spectrum shows the disappearance of the NC*H*N proton after exposure during 2 min to UV radiation (365 nm, 65 mW·cm^{-2}). In addition, reaction of the two as-irradiated media with CS_2 gives the expected **1**-CS_2 and **2**-CS_2 complexes whose structures have been identified by ^{13}C NMR (Fig. S1 of Supporting Information). These characterizations suggest deprotonation of the two azolium salts to form the expected NHCs **1** and **2**. Given the high reactivity of NHCs, it is however important to develop new techniques able to characterize these species just after their formation, i.e. before secondary reactions take place. Recently, the fast addition of a radical to NHC to afford an adduct with an unpaired electron was evidenced by Tumanskii et al.[40,41] Through a judicious choice of radicals, it was possible to generate adduct radicals stable enough to be detected by ESR spectroscopy, thus providing a clean spectrum characteristic of the carbene captured. Following the same approach, we chose diphenyl(2,4,6-trimethylbenzoyl)phosphine oxide (TPO) to act as a trapper of NHCs just after their photogeneration. TPO is a commercial *α*-cleavable radical photoinitiator, which was not reported by Tumanskii et al. It proceeds through the photochemical homolysis of the C-C bond adjacent to the arylketone chromophore to yield two different phosphinoyl- (**P$^\bullet$**) and mesitoyl-type (**M$^\bullet$**) radicals (**Scheme 2**). The main advantage is that these radicals can be photogenerated at the same wavelength (365 nm) as the NHC, allowing the NHC to be trapped as a well-defined adduct radical in a single step, and immediately after generation. The mixture **1H$^+$BPh$_4^-$**/ITX (3/1 equiv.) was irradiated in THF in presence of TPO (6 equiv.), then placed after different exposure times, in the cavity of the ESR spectrometer.

As shown in **Figure 2**, the ESR spectrum recorded after 2 min irradiation, is consistent with the formation of a single adduct radical, which was assigned to **1$^\bullet$-M**. Indeed, the spectrum clearly shows a quintuplet arising from the hyperfine coupling (hfc) of the unpaired electron with two equivalent ^{14}N atoms (I = 1, a_N = 3.9 G). Because of coupling with the two protons of the **1** moiety (I = ½, a_H = 1.1 G), each quintet line is also decomposed, but only in doublet instead of triplet, because the set of hfc transitions are probably overlapped. The formation of the phosphinoyl radical adduct **1$^\bullet$-P** can be ruled out because hfc with ^{31}P (I = ½) would have caused a duplication of the

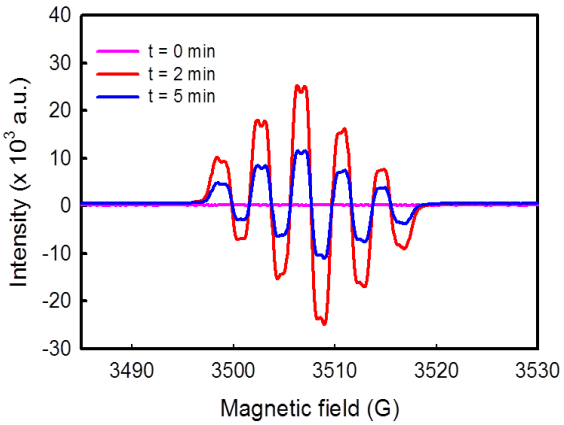

Figure 2. ESR spectrum of a solution of ITX/**1H$^+$BPh$_4^-$**/TPO (1/3/6 equiv., [ITX] = 5 × 10^{-3}M) in THF after different irradiation times.

quintuplet. Control experiment by irradiating the preformed NHC **1** and TPO for 30 s reveals a similar profile (Fig. S2), thus supporting the photoinduced liberation of **1** in the previous experiment and the *in situ* formation of a single NHC adduct radical. This latter result can be explained through DFT calculations since the addition reaction of the **M$^\bullet$** radical to **1** is much more exothermic (△H = -35.0 kcal·mol^{-1}) than that of a **P$^\bullet$** radical (△H = -17.1 kcal·mol^{-1}) as expected from the higher stability of the **1$^\bullet$-M** (Fig. S3). Nevertheless, the ESR spectrum shows a signal intensity declining with longer exposure time (see t = 5 min, **Figure 2**), in line with a slow degradation of the **1$^\bullet$-M** adduct radical under UV irradiation. This result was also confirmed when **1$^\bullet$-M** adduct was created from the preformed NHC **1** instead of the photoNHC (Fig. S2).

^{1}H NMR analysis of NHC-carbodiimide adduct: Quantification of NHC. Estimation of the quantity of NHC photogenerated from the mixture of azolium salt with excited ITX can be challenging. ^{1}H NMR provides a deprotonation degree (from NC*H*N proton), but the results can be distorted when the reaction is not complete because of N-CH-N/N-C:-N hydrogen bonds forming in **1H$^+$-1** complex (see evidences in Fig. S4). Alternatively, NHC concentration can be determined indirectly through a quantitative reaction between **1** and CS_2.[36] However, the zwitterionic **1**-CS_2 adduct is only partially soluble in solvents such as THF and acetonitrile, making yield calculation complex because the adduct is partitioned between solid and liquid phases. To obtain quantitatively a soluble and stable NHC adduct, we turned our attention towards the recently reported NHC-carbodiimide (CDI) adduct[42,43] generated by addition of a CDI derivative to **1** (**Scheme 3**). Upon contact with a stoichiometric amount of 1,3-di-*p*-tolylcarbodiimide in THF, **1**

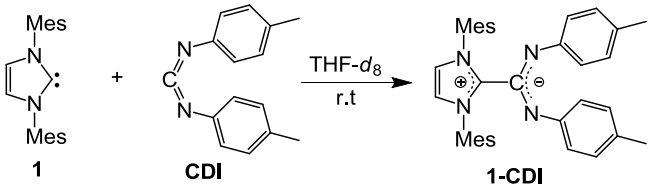

Scheme 3. Formation of zwitterrionic **1**-CDI adduct by reaction between CDI and NHC **1**.

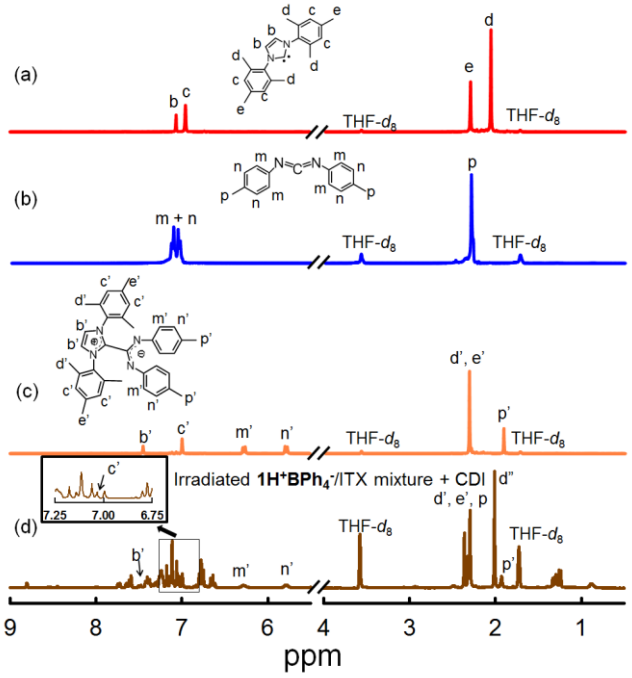

Figure 3. ^{1}H- NMR spectra in THF-d_8 of: (**a**) **1** (0.21 M), (**b**) CDI (0.21 M), (**c**) **1**/CDI, (1/1 equiv., [**1**] = 0.1 M), and (**d**) **1H$^+$BPh$_4^-$**/ITX/CDI (3/1/3 equiv., [ITX] = 0.01 M). In sample **d**, **1H$^+$BPh$_4^-$**/ITX was irradiated 5 min then CDI was immediately added.

yields a soluble carbene adduct within a few seconds, visible by the change of color from a slight yellow solution to orange. The product formed in this way was characterized by ^{1}H NMR when the reaction was performed in THF-d_8 (**Figure 3**). The reaction caused a complete shift of the methyl protons H_e (2.31 ppm) and H_d (2.08 ppm,) of **1** (spectrum **a**) and the methyl proton H_p (2.30 ppm) of CDI (spectrum **b**). In the spectrum of the mixture **1**/CDI (spectrum **c**), $H_{e'}$ and $H_{d'}$ form two overlapping peaks at 2.32 ppm, and $H_{p'}$ is subjected to a upfield shift and now arises at 1.92 ppm. Additionally, novel signals assigned to methine protons $H_{m'}$ (6.27 ppm) and $H_{n'}$ (5.77 ppm) appear in the spectrum, which established the quantitative transformation of **1** to the **1**-CDI adduct.

Another control experiment was performed when **1** (1 equiv.) was mixed with **1H$^+$BPh$_4^-$** (3 equiv.) followed by addition of CDI (1 equiv.). It cleanly gave a yield of **1**-CDI consistent with the initial amount of **1** (with an error of 5 %, Fig. S4), demonstrating that this reaction may also cause the disruption of the **1H$^+$**-**1** hydrogen bonds.[44–46] Having proved that the synthesis of NHC-CDI can be quantitative and easily monitored by ^{1}H NMR, 1,3-di-*p*-tolylcarbodiimide was added to the as-irradiated solutions of **1H$^+$BPh$_4^-$**/ITX and **2H$^+$BPh$_4^-$**/ITX (3/1 equiv.). As expected, the spectrum **d** of this mixture (**Figure 3**) displays all the characteristics resonances of **1**-CDI adduct, enabling to determine NHC conversion. After 5 min irradiation, the yields of **1** and **2** were respectively of 22.1 and 14.8 %. The main factor underlying this trend and the best experimental conditions to achieve high NHC yield are discussed in next sections.

2. Insight into photochemical mechanism: coupled electron/proton transfer

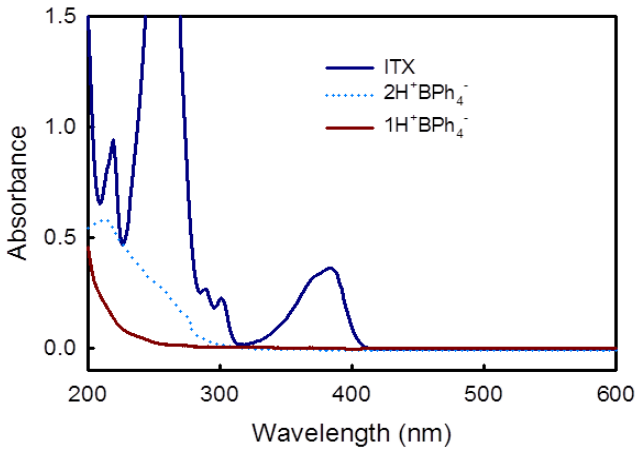

Figure 4. UV spectra of ITX, **1H$^+$ BPh$_4^-$** and **2H$^+$ BPh$_4^-$** in acetonitrile ([ITX] = 10^{-4} M, [**1H$^+$BPh$_4^-$**] = [**2H$^+$BPh$_4^-$**] = 3×10^{-4} M).

UV-Vis Absorption. **Figure 4** shows in the same plot the UV-vis spectra of ITX, **1H$^+$BPh$_4^-$** and **2H$^+$BPh$_4^-$** in acetonitrile. ITX has an absorption spectrum with two characteristic maxima at 257 nm (π-π* transition) and 383 nm (n-π* transition). The band centered at 383 nm allows excitation (λ_{exc} = 365 nm) to form triplet ITX (^{3}ITX*), displaying a much higher reduction ability than its ground state analogue. The two azolium salts absorb only in the UVC range (100-280 nm), what is desired to avoid electronic excitation and ensure high reactivity of ITX.

Real-time photobleaching and Rehm-Weller equation. The decay of the ITX n-π* transition band at 365 nm was assessed throughout irradiation time with a rapid-scan spectrometer, which is able to measure absorbance change with a temporal resolution of 0.1 s. To investigate the photochemical mechanism, real-time photobleaching was performed in acetonitrile during 50 s for a range of ITX/quencher couples (**Figure 5**). The first series (**a**) displays azolium salts bearing anions with different electron donor properties (Cl^- and BPh_4^-), while the second (**b**) shows tetraphenylborate salts containing different cations (**1H$^+$**, **2H$^+$** and Na^+). As expected, a control experiment including only ITX showed a steady absorbance value over irradiation (**Figure 5a**), within the time period studied, suggesting its photostability in absence of suitable reductant.[47] This is in sharp contrast with the profile of **1H$^+$BPh$_4^-$**/ITX which shows a gradual photobleaching, consistent with a modification of the structure of ITX after the electron-transfer reaction. Indeed, $\triangle G_{et,1HBPh4}$, the free energy change of electron-transfer from BPh_4^- to ^{3}ITX* is slightly negative (-0.07 eV, see calculation details in SI), showing that the reaction is thermodynamically feasible. Furthermore, it is the irreversible process since the back electron-transfer of the boronyl radical $^\bullet BPh_4$ may be prohibited by its homolytic cleavage into BPh_3 and $Ph^\bullet$ within the femto-second time scale.[48] A number of evidences are consistent with this hypothesis of sensitized reaction (**Scheme 4**). With **1H$^+$Cl$^-$**, it is explicit that ITX does not photobleach due to the lack of electron donating ability of Cl^-, as exemplified by the absence of oxidation potential during electrochemical measurements.

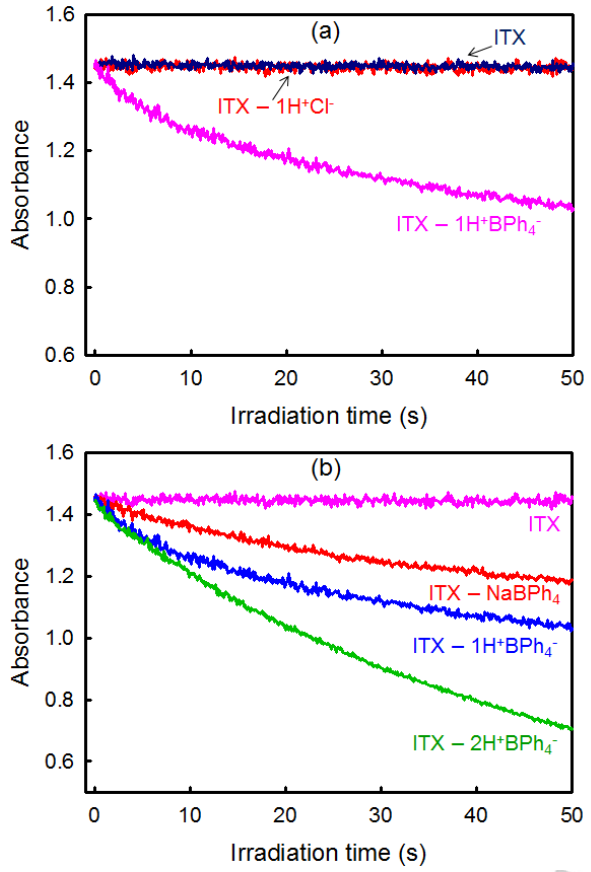

Figure 5. Photobleaching kinetics of ITX (2×10^{-4} M in acetonitrile) monitored at 365 nm in the presence of different quenchers: azolium salts (**a**) and tetraphenylborate salts (**b**) (Quencher concentration is 6×10^{-4} M).

On the other hand, useful and complementary results about the second step of proton transfer can be gained by the photobleaching of ITX in presence of various tetraphenylborate salts (**Figure 5b**). Whatever the cation (**1H**$^+$, **2H**$^+$, Na^+), a bleaching of ITX is observed which is consistent with the irreversible electron-transfer reaction involving BPh_4^-, but the photolysis rates are clearly different. $NaBPh_4$ induces the lowest rate of photobleaching (1.58×10^{-7} M·s^{-1}), compared to **1H$^+$BPh$_4^-$** (2.40×10^{-7} M·s^{-1}) and **2H$^+$BPh$_4^-$** (4.04×10^{-7} M·s^{-1}) even the $\triangle G_{et,NaBPh4}$ value is slightly more negative ($\triangle G_{et,NaBPh4}$ = -0.18 eV). One possible explanation for the differences of ITX decomposition rate could be the slower electron-transfer rate of $NaBPh_4$ compared to other borate salts.[36]

Besides, with azolium salts, proton transfer can occur leading to the formation of NHCs which are known to be excellent electron donors. Therefore, a secondary reaction involving electron-transfer from the as-formed NHC with excited ITX is likely to occur to give a carbene radical cation **1**$^{\bullet+}$ (or **2**$^{\bullet+}$) and ITX radical anion (**Scheme 5**). Transient species **1**$^{\bullet+}$ (or **2**$^{\bullet+}$) could undergo a dimerization to form a bicationic product or regeneration of azolium cations.[49] Supporting this hypothesis, electron-transfer between carbene **1** or **2** and the triplet ITX is strongly exergonic ($\triangle G_{et,1}$ = -1.85 eV and $\triangle G_{et,2}$ = -2.53 eV) because the oxidation potentials of **1** and **2** are very low, -0.84 V and -1.52 V vs. SCE, respectively. Moreover, neat electron-

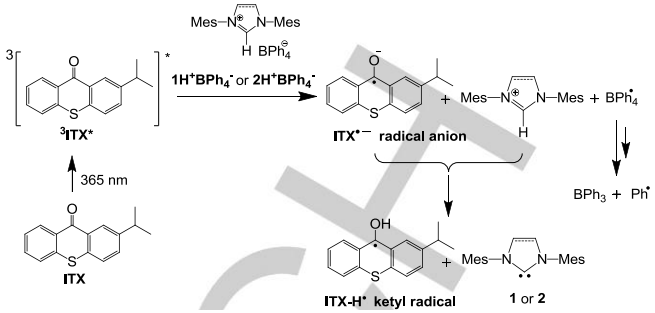

Scheme 4. Photochemical mechanism for the generation of NHC **1** and **2** combining electron-transfer and proton transfer.

transfer between **1** (or **2**) and ^{3}ITX* was evidenced by photobleaching rate of ITX in the presence of **1** and 2 with significant rates, 3.6×10^{-8} M·s^{-1} and 9.8×10^{-8} M·s^{-1}, respectively (Fig. S5). Thereby, with the two azolium salts, faster decomposition rates (**Figure 5b**) may be thus driven by triplet ITX electron-transfer reactions occurring not only with BPh_4^- but also with the NHC formed. In agreement with this hypothesis, the photolysis rate of **2H$^+$BPh$_4^-$** is approximately twice as large as that of **1H$^+$BPh$_4^-$** which is consistent with the better electron donating properties of imidazolinylidene **2** compared to its imidazolylidene counterpart **1**.

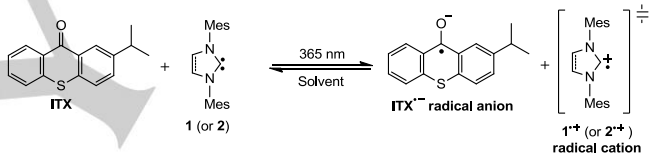

Scheme 5. Photoreduction of ITX by **1** (or **2**) generates NHC radical cations.

3. Optimization of NHC yield

Effect of ITX concentration. As discussed above, it is known that ^{3}ITX* is not only involved in electron-transfer with BPh_4^-, but also with photogenerated **1** (or **2**) leading to the degradation of the desired carbene under irradiation. Therefore, it is crucial to investigate the influence of ITX concentration on the yield of photogenerated NHC. For this purpose, the influence of the ITX/**1H$^+$BPh$_4^-$** molar ratios (0 - 1.33) was assessed while maintaining the irradiation conditions unchanged (5 min, 65 mW·cm^{-2}). As can be seen in **Figure 6**, the increase of the

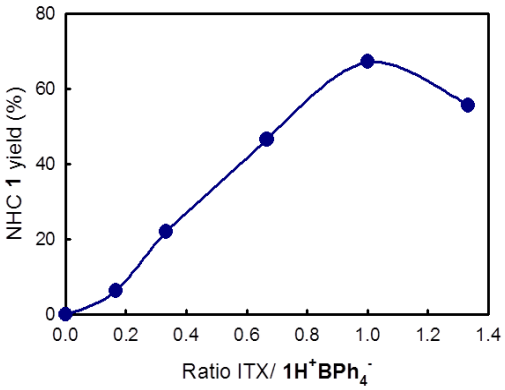

Figure 6. Effect of ITX concentration on NHC **1** yield produced by irradiation of ITX/**1H$^+$BPh$_4^-$** ([**1H$^+$BPh$_4^-$**] = 0.03 M). Irradiation conditions: 65 mW·cm^{-2}, 5 min.

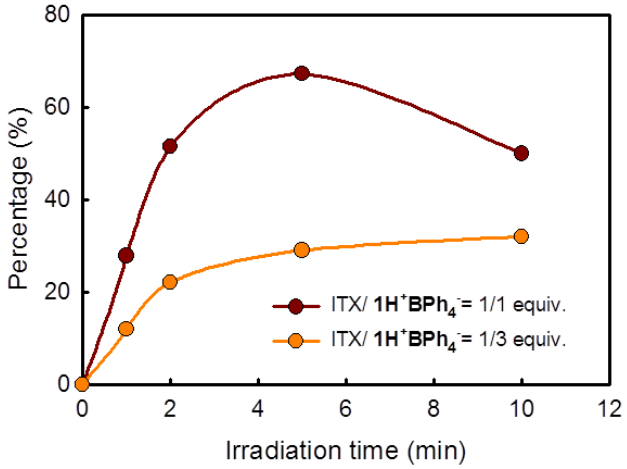

Figure 7. Effect of irradiation time on NHC **1** yield following the photolysis of ITX/**1H$^+$BPh$_4^-$** mixture ([**1H$^+$BPh$_4^-$**] = 0.03 M). Irradiation conditions: 365 nm, 65 mW·cm^{-2}.

ITX/**1H$^+$BPh$_4^-$** ratio, until stochiometry is reached, results in a nearly linear increase of **1** yield. A maximum amount of 70 % can be generated upon using a stochiometric ratio. However, further increase of ratio ITX/**1H$^+$BPh$_4^-$** causes the yield to slightly decrease (56 %). Presumably, a higher concentration in ITX contributes to more side reactions between **1** and ^{3}ITX*.

Effect of irradiation time. The effect of irradiation time on **1** yield is illustrated in **Figure 7**. Using a sub-stoichiometric ratio in ITX (ITX/**1H$^+$BPh$_4^-$** = 1/3), a gradual release of **1** is observed within 5 min, then the yield levels off at 30 %. Because ITX is in sub-stoichiometry, photodegradation can be minimized, but at the same time, only moderate yields can be achieved. The kinetic profile is significantly changed upon increasing the concentration of ITX to reach stoichiometry (ITX/**1H$^+$BPh$_4^-$** = 1/1 equiv.). Under these conditions, more NHC can be released because of the higher ^{3}ITX* concentration, and a maximum of 70 % is formed after 5 min. However, after longer radiation exposure, there is now a significant decrease of **1** yield (56 % after 10 min) due to the photochemical degradation of **1** by ^{3}ITX*.

Effect of photooxidant. The influence of other aryl ketone photooxidants than ITX on NHC yield was estimated using thioxanthone (TX), 4,4′-bis(diethylamino)benzophenone (EAB) and camphorquinone (CQ) (**Table 1**).

Table 1. Effect of the photooxidant's nature on the release of photogenerated NHC **1**. **1H$^+$BPh$_4^-$**/Photooxidant (3/1 equiv.) was irradiated in C_4D_8O ([Photooxidant] = 0.03 M). Irradiation conditions: 365 nm, 65 mW·cm^{-2}, 5 min irradiation).

Entry	Photooxidant	Structure	NHC 1 yield[a] (%)
a	ITX	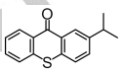	22
b	TX		24
c	EAB	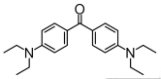	0
d[b]	CQ		0

[a] Determined by ^{1}H-NMR spectroscopy after CDI addition. [b] Irradiation with a 450 nm LED (55 mW·cm^{-2})

As expected, the nearly similar redox properties of excited ITX (*entry a*) and TX (*entry b*) resulted in a comparable amount of **1** released, 22 % and 24 %, respectively. Conversely, the replacement of ITX by EAB (*entry c*) and CQ (*entry d*) prevents the formation of **1**. In accordance with this result, the electron-transfer between BPh_4^- and the excited state of these two electron donors was found to be non-thermodynamically favorable ($\triangle G_{et,\ EAB}$ = 0.44 eV, $\triangle G_{et,\ CQ}$ = 0.07 eV).[50,51]

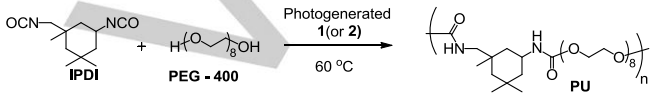

Scheme 6. Synthesis of polyurethane catalyzed by photogenerated NHC.

4. Use of NHC photogenerator in polymerization

Synthesis of polyurethane. There have been very few studies utilizing NHC organocatalyst in PU polymerizations in the literature.[16,24] Nevertheless, NHC photogenerators were evaluated in the model linear step-growth polymerization of isophorone diisocyanate (IPDI) and poly(ethylene glycol) (M_n = 400 g·mol^{-1}, PEG_{400}) (**Scheme 6**). Through a possible alcohol activation mechanism (Scheme S1),[16,52] a polymerization was accomplished at 60°C by mixing a stoichiometric amount of PEG_{400} and IPDI followed by addition of the photogenerated NHC (0.3 mol %). **Table 2** summarizes yield, molecular weight and polydispersity (*Đ*) after 4 h for each polymerization using **1H$^+$BPh$_4^-$**/ITX (*entry a*) or **2H$^+$BPh$_4^-$**/ITX (*entry b*). For comparative purposes, the free NHC **1** (***entry a'***) was also included as polymerization control as well as an uncatalyzed reaction (*entry c*).

Without catalyst, full conversion was not reached and a low molecular weight polyurethane was obtained (M_n = 1700 g·mol^{-1}, *entry c*). In contrast, the two photoNHCs (*entry a-b*) exhibited

Table 2. Results of step-growth polymerization of PEG_{400}/IPDI (342/342 equiv.). Reactions were conducted for 4 h at 60°C after the addition of the as-irradiated azolium salt/ITX solution (1/1 equiv.) or free NHC (1 equiv.).

Entry	Catalyst system	M_n[a] (g·mol^{-1})	M_w[b] (g·mol^{-1})	*Đ*[c]	T_g[d] (°C)	Yield[e] (%)
a	**1H$^+$BPh$_4^-$**/ITX	4900	7800	1.59	-17	95.7
a'	**1**	5100	7900	1.55	-14	98.3
b	**2H$^+$BPh$_4^-$**/ITX	4100	6800	1.67	-18	96.2
c	No catalyst	1700	4700	2.69	-23	40.1

[a] Experimental number average molar mass M_n obtained by SEC. [b] Experimental weight average molar mass *M*w obtained by SEC. [c] Polymer dispersity index *Đ*= M_w/ M_n. [d] Glass transition temperature determined by DSC. [e] Isolated yield.

greater polymer yields (> 95 %), higher molecular weights (4000 - 5000 g·mol^{-1}) and lower dispersity values *Đ* in the range from

1.5 to 1.7 (see SEC traces in Fig. S6). Consistently, the control experiment using the preformed NHC **1** (*entry a'*) resulted in polymers displaying similar M_n, $Đ$ and glass transition temperature. Although the molecular weights are moderate, these results demonstrate the role of (photo)NHC in the catalysis of the polymerization. To more precisely compare catalytic activities, kinetic studies were performed for **1** and **1H$^+$BPh$_4^-$**/ITX during the first hour of reaction (**Figure 8**). The two catalysts proceeded at relatively similar rates with a significant acceleration compared to the uncatalyzed experiment. The slightly slower kinetics for photogenerated **1** was assigned to lower amount of NHC **1** present in the reaction media (as compared to the preformed-NHC **1**) since a maximum yield of 70 % in released NHC can be reached as demonstrated before.

Synthesis of polyester. Encouraged by this first result, the NHC photogenerator's catalytic activity was also evaluated in ring-opening copolymerization (ROCOP) of epoxide and anhydride. This reaction offers a controlled route to polyesters, although it has been much less studied than ring-opening polymerization of cyclic esters.[53,54] ROCOP generally requires organometallic initiators to reach efficient curing, but the use of NHC was reported very recently.[55,56] In a model copolymerization, the as-irradiated azolium salt/ITX mixture (1/1 equiv.) was added to a mixture of cyclohexene oxide (CHO, 500 equiv.) and phthalic anhydride (PA, 100 equiv.) (**Scheme 7**). Polymerization was conducted at 110°C using thus CHO as both the monomer and the solvent.

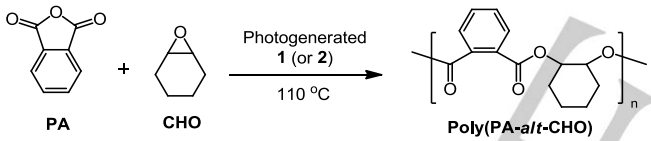

Scheme 7. ROCOP of PA and CHO using photogenerated NHC **1** and **2** as catalyst.

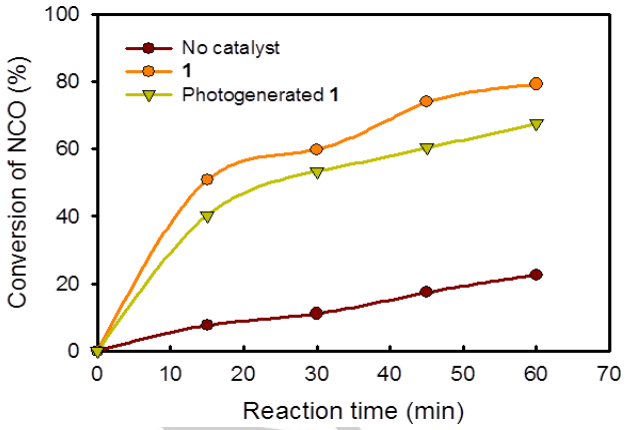

Figure 8. NCO conversion during polyaddition reaction between PEG_{400} and IDPI. Conversion values were determined based on the NCO stretching band (υ_{-NCO}) at 2255 cm^{-1} using CH_2 symmetric stretch at 2870 cm^{-1} as reference (see FTIR spectra in Fig. S7). NCO conv. (%) = $\frac{A_t - A_0}{A_0}$ × 100 where A_0 and A_t are the integrated absorbance at 2255 cm^{-1} corresponding to reaction time at 0 min and t min.

Table 3. Results of ROCOP of CHO/PA (500/100 equiv.). Polymerization were conducted at 110°C for 60 min in THF after the addition of the as-irradiated azolium salt/ITX solution (1/1 equiv.) or free NHC (1 equiv.).

Entry	Catalyst system	PA conv.[a] (%)	Ester conv.[b] (%)	$M_{n\text{-SEC}}$[c] (g·mol^{-1})	$Đ$[d]
a	**1H$^+$BPh$_4^-$**/ITX	98	> 95	3800	1.21
a'	**1**	92	> 95	3000	1.16
b	**2H$^+$BPh$_4^-$**/ITX	84	> 95	3500	1.18
c	No catalyst	0	-	-	-
d	NaBPh$_4$/ITX	0	-	-	-

[a] Determined by ^{1}H-NMR. PA conv.(%) = $\frac{I_{7.85-8.02}}{I_{7.85-8.02} + I_{7.31-7.62}}$ × 100 where $I_{7.85-8.02}$ is the intensity of methine protons (δ_a= 7.85 – 8.02 ppm) of residual PA and and $I_{7.31-7.62}$ is the intensity of methine protons (δ_b= 7.31 – 7.62 ppm) of poly(PA-*alt*-CHO) (Fig. S8). [b] Percentage of ester linkages in isolated poly(PA-*alt*-CHO) calculated by ^{1}H-NMR in DMSO-d_6 (Fig. S9) and MALDI-ToF (Fig. S10). [c] Experimental number average molar mass M_n obtained by SEC. [d] Polymer dispersity index $Đ = M_w/M_n$ obtained by SEC.

Table 3 shows PA conversion, molecular weight and polydispersity ($Đ$) after 1 h reaction using **1H$^+$BPh$_4^-$**/ITX (*entry a*) or **2H$^+$BPh$_4^-$**/ITX (*entry b*) along with two control experiments (entries *c-d*). As expected, no reaction took place in the uncatalyzed control reaction (*entry c*).[55] Conversely, almost full conversions were achieved with **1H$^+$BPh$_4^-$** (98 %) and with **2H$^+$BPh$_4^-$** (84 %). In addition, the polyesters produced exhibited a highly alternating structure with a high fraction of ester linkages (> 95 %, see ^{1}H NMR spectra in Fig. S9). By contrast, it is well-known that conventional catalytic systems such as metalloprophyrin or salen can form a significant proportions of ether linkages resulting from CHO homopolymerization.[53,54] The alternating structure was also evidenced in the MALDI-ToF MS spectrum of polymer *a* (Fig. S10) which displayed an m/z increment of 246.26 g·mol^{-1} corresponding to the exact molar mass of the [PA + CHO] repeating unit. Interestingly, no IMes end-capped chains were identified due to quenching of the reaction mixture in methanol. As a result, the five main populations of peaks were all assigned to α-methyl-ω-hydroxyl OH/CH_3-terminated polymers. The mechanism was presumed to proceed through a nucleophilic attack of NHCs on anhydride functionality (Scheme S2).[55,56] Besides, copolymers *a* and *b* exhibited monomodal SEC traces with narrow molecular weight distributions ($Đ$ ~ 1.2, see Fig. S11). Surprisingly, **1H$^+$BPh$_4^-$** showed slightly higher conversions and M_n values than **1** despite incomplete deprotonation, raising doubts about the role of other photoproducts in reaction catalysis. However, the replacement of **1H$^+$BPh$_4^-$** by $NaBPh_4$ afforded no polymer (*entry d*).

Synthesis of polynorbornene. In the field of catalyst precursors for olefin metathesis, NHC-coordinated ruthenium complexes with the general formula $RuCl_2$(arene)(NHC) stand out by their ease of preparation. They can be produced *in situ* from commercial and inactive ruthenium dimers such as [$RuCl_2$(*p*-cymene)]$_2$ (**Scheme 8**) after addition of a suitable free

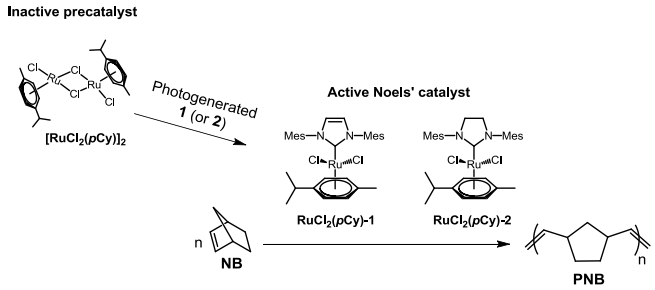

Scheme 8. Strategy for *in-situ* formation of $RuCl_2$(*p*-cymene)NHC from the inactive precatalyst $[RuCl_2(p\text{-cymene})]_2$ dimer and photogenerated NHC **1** and **2**. The active NHC-coordinated Ru complexes referred to as Noels' catalysts can be used as active for the ROMP of NB

NHC such as **1** or **2**, which causes the dissociation of this precatalyst.[57,58] The resultant active complexes, $RuCl_2$(*p*-cymene)-**1** or $RuCl_2$(*p*-cymene)-**2**, have emerged as versatile and efficient catalysts to promote the ROMP of both strained and low ring-strained cyclic olefins.[59–61] Building on our previous study,[36] we show herein that it is possible to generate *in situ* the active $RuCl_2$(*p*-cymene)NHC complex bearing ligand **1** or **2**,[59,60,62] by irradiation of the NHC photogenerator ITX/**1H$^+$BPh$_4^-$** (or ITX/**2H$^+$BPh$_4^-$**) in presence of the ruthenium precatalyst $[RuCl_2(p\text{-cymene})]_2$. Using this 3-component system, it is thus possible to trigger the ROMP of cyclic olefins such as norbornene (NB) under UV exposure.

The catalytic activity of the three-component system $[RuCl_2(p\text{Cy})]_2$/**1H$^+$BPh$_4^-$**/ITX (1/5/2.5 equiv.) for the ROMP of norbornene in CD_2Cl_2 was evaluated. In contrast to previous experiments where the as-irradiated photoNHC/ITX was introduced later, NHC photogenerator was initially present in the reaction medium and polymerizations were conducted at room temperature. **Table 4** displays NB conversion, molecular weight and *cis* content after 1 min reaction at ambient temperature. As expected, the irradiation of a solution devoid of Ru dimer results in no reaction (*entry a*). Without photoNHC (*entry b*), a very small conversion was detected (< 2%). By contrast, much higher conversion (78 %) was achieved using the 3-component mixture $[RuCl_2(p\text{Cy})]_2$/**1H$^+$BPh$_4^-$**/ITX (*entry c*) suggesting the successful formation of the highly active ruthenium-arene complex bearing an NHC ligand. Replacing **1H$^+$BPh$_4^-$** by **2H$^+$BPh$_4^-$** resulted in similar conversions (76 %, *entry d*), molecular weight and *Đ* (Fig. S12). It is well established in the literature that the unsaturation in the imidazole ring of NHC moiety is not a crucial feature altering catalytic efficiency.[61] In both cases, σ_{cis} (≈ 40-50 %) was very similar to that found in the corresponding polymer prepared by the action of a Ru–NHC complex,[61,63] thereby suggesting the formation of the same ROMP catalyst. As control experiments, we also conducted the polymerization of NB utilizing a combination of Ru precatalyst with free NHC **1**. In the dark, the mixture of $[RuCl_2(p\text{-cymene})]_2$ and **1** resulted in slightly lower monomer consumption (58.9 %, *entry e*) after 1 min of reaction. This result supports the hypothesis that radiation facilitates the decoordination of the *p*-cymene ligand to form an active species.[59]

Table 4. Results for the photoROMP of NB conducted at ambient conditions by 1 min irradiation (365 nm, 6.5 mW·cm^{-2}) of the mixture NB/Ru dimer/photoNHC/ITX in CD_2Cl_2 (510/1/5/2.5 equiv., [NB] = 1 M).

Entry	photo-NHC	Ru dimer/ photoNHC/ ITX (equiv.)	Conv.[a] (%)	σ_{cis}[b]	$M_{n\text{-th}}$[c] (kg·mol^{-1})	$M_{n\text{-SEC}}$[d] (kg·mol^{-1})	$Đ$[e]
a	**1H$^+$BPh$_4^-$**	0/5/2.5	0	n.d	n.d	n.d	n.d
b	**-**	1/0/0	1.5	9.3	0.36	n.d.	n.d.
c	**1H$^+$BPh$_4^-$**	1/5/2.5	78	51.9	18.69	146.8	3.02
d	**2H$^+$BPh$_4^-$**	1/5/2.5	76	42.5	18.00	138.3	3.14
e	**1**	1/2[f]/0	59	59.4	14.11	319.2	3.70

[a] Determined by ^{1}H-NMR NB conv.(%) = $\frac{I_{5.21}+I_{5.36}}{I_{5.21}+I_{5.36}+I_{5.99}} \times 100$ where $I_{5.21}$ and $I_{5.36}$ are the intensity of vinylic protons (δ= 5.21 ppm and δ= 5.36 ppm) of polynorbornene and $I_{5.99}$ is the intensity of vinylic proton (δ= 5.99 ppm) of residual NB. [b] *Cis* content of the polymers calculated from ^{1}H-NMR spectrum *cis* (%) = $\frac{I_{5.36}}{I_{5.21}+I_{5.36}} \times 100$. [c] Theoretical number average molar mass $M_{n\text{-th}}$ = $\text{Conv.} \times \frac{[NB] \times M_{NB}}{2 \times [\text{Ru dimer}]}$. [d] Experimental number average molar mass M_n obtained by SEC. [e] Polymer dispersity index $Đ$= M_w/ M_n obtained by SEC. [f] The solution was kept in dark for 1 min, n.d. means not determined due to no polymerization or insoluble polymer.

Conclusions

In presence of ITX, imidazolium or imidazolinium salts bearing tetraphenylborate as anion are able to generate photochemically the corresponding free imidazolylidene and imidazolidinylidene species upon irradiation at 365 nm. The mechanism has been investigated by means of steady-state photolysis. It involves a first electron-transfer reaction from the easily oxidized electron donor BPh_4^- to excited ITX acting as an electron acceptor. The thioxanthone radical anion formed can then abstract a proton from the azolium cation to yield the free NHCs. The formation of the NHCs, IMes (**1**) and SIMes (**2**), was proved by ESR spectroscopy in THF through the formation of a persistent NHC-mesitoyl radical adduct. A maximum amount of NHC of 70 % was produced in THF, based on the azolium cation precursor, as determined by ^{1}H-NMR of a stable and soluble NHC-CDI adduct. Irradiation time should be carefully controlled to avoid overexposure resulting in secondary electron-transfer reaction between triplet ITX and the NHC formed. The easy synthesis of NHC progenitors **1H$^+$BPh$_4^-$** and **2H$^+$BPh$_4^-$** opened the way to novel photomediated polymerization reactions where NHCs advantageously acted as organocatalysts in place of metals. Linear polyurethanes were synthesized by the step-growth polymerization of diols and diisocyanate. Additionally, the ring-opening copolymerization of anhydride with epoxy yielded polyesters with narrow polydispersity. Finally, in combination with an inactive Ru precatalyst, photolatent NHCs could also drive the formation of highly active ruthenium-NHC complexes for ring-opening polymerizations of norbornene with > 76 % conversion reached after 1 min of irradiation. It is expected that a wide variety of other NHC-mediated organic chemical reactions and polymerization reactions could benefit from this innovative NHC photogenerating system; in particular, those including thermally sensitive substrates or requiring a spatial control.

Experimental Section

1. Materials

1,3-Bis(mesityl)imidazolium chloride (**1H$^+$Cl$^-$**, 98 %), sodium tetraphenylborate ($NaBPh_4$, 99.5 %), diphenyl(2,4,6-trimethylbenzoyl)phosphine oxide (TPO, >98%), isophorone diisocyanate (IPDI, 99.0 %), polyethylene glycol 400 g·mol^{-1} (PEG_{400}), and vinyl ethyl ether (> 98.0 %) were purchased from TCI. 1,3-Bis(mesityl)imidazole-2-ylidene (**1**, 97 %), 1,3-bis(mesityl)imidazolidin-2-ylidene (**2**, 97 %), 1,3-bis(mesityl)imidazolinium chloride (**2H$^+$Cl$^-$**, 98 %), acetonitrile-d_3 (CD_3CN, 99.8 % D), isopropyl-9H-thioxanthen-9-one, mixture of 2-and 4-isomers (ITX, 97%), 1,3-di-*p*-tolylcarbodiimide (CDI, 96 %), 4,4′-bis(diethylamino)benzophenone (EAB, > 99 %), camphorquinone (CQ, 98 %), phthalic anhydride (PA, > 99 %), cyclohexene oxide (CHO, 98%) and dichloromethane were obtained from Sigma Aldrich. Dichloromethane-d_2 (CD_2Cl_2, 99.5 % D), tetrahydrofuran-d_8 (THF-d_8, 99.5 % D), chloroform-d_1 ($CDCl_3$, 99.5 % D) and dimethyl sulfoxide-d_6 (DMSO-d_6, 99.5 % D) were bought from Eurisotop. Dichloro(*p*-cymene)ruthenium(II) dimer ($[RuCl_2(p\text{-cymene})]_2$, 98 %), was obtained from Strem Chemicals. Other HPLC grade solvents such as ethanol, acetonitrile and tetrahydrofuran (THF) were received from VWR. All the solvents and CHO were distilled and stored over molecular sieve (4 Å) under nitrogen atmosphere before use.

2. Synthesis

2.1 Synthesis of azolium tetraphenylborate salts. **1H$^+$BPh$_4^-$** and **2H$^+$BPh$_4^-$** were prepared following a procedure published elsewhere.[36] ^{1}H-NMR (300 MHz, CD_3CN), **1H$^+$BPh$_4^-$**, isolated yield 93.2 % : δ_{ppm} : 2.14 (s, 12H, 4 × *o*-ArC*H*$_3$), 2.42 (s, 6H, 2 × *p*-ArC*H*$_3$), 6.85 – 6.89 (t, 4H, *J* = 6 Hz, 4 × Ar*H*), 6.99 – 7.04 (t, 8H, *J* = 7.5 Hz, 8 × Ar*H*), 7.2 (s, 4H, 4 × Ar*H*), 7.30 – 7.34 (br, 8H, 2 × 8 × Ar*H*), 7.56 (s, 2H, 2 × NC*H*) and 8.63 (s, 1H, NC*H*N). **2H$^+$BPh$_4^-$**, isolated yield 84 % : δ_{ppm} : 2.36 (s, 6H, 4 × *p*-ArC*H*$_3$), 2.37 (s, 12H, 2 × *o*-ArC*H*$_3$), 4.34 (s, 4H, 2 × NC*H*$_2$), 6.86 – 6.91 (t, 4H, *J* = 7.5 Hz, 4 × Ar*H*), 7.01 – 7.06 (t, 8H, *J* = 7.5 Hz, 8 × Ar*H*), 7.12 (s, 4H, 4 × Ar*H*), 7.31 – 7.36 (br, 8H, 2 × 8 × Ar*H*), and 8.07 (s, 1H, NC*H*N).

2.2 Synthesis of polyurethane. A spectroscopic cell capped with a rubber septum was charged with **1H$^+$BPh$_4^-$** (9.18 mg, 0.015 mmol, 1 equiv.), ITX (3.82 mg, 0.015 mmol, 1 equiv.) and 0.5 mL of THF. A Schlenk tube containing the diol oligomer PEG_{400} (2050 mg, 5.125 mmol, 342 equiv.) and diisocyanate IPDI (1139 mg, 5.125 mmol, 342 equiv.) was subjected to three freeze-thaw cycles. The cuvette containing the NHC photogenerator solution was degassed, then exposed to a 365 nm LED irradiation (65 mW·cm^{-2}) for 5 min. The solution that turned dark brown color was added under inert atmosphere to the Schlenk tube. The step-growth polymerization was carried out at 60°C for 4 h. The progress of the reaction was monitored by FT-IR by taking occasional samples. The polymer was terminated by methanol and precipitated in cyclohexane, filtered under vacuum and dried under vacuum at 60 °C until a constant weight was achieved. The resultant polymer was then analyzed by SEC.

2.3 Synthesis of polyester. A spectroscopic cell capped by a rubber septum was charged with **1H$^+$BPh$_4^-$** (9.18 mg, 0.015 mmol), ITX (3.82 mg, 0.015 mmol) and 0.5 mL of THF. A Schlenk tube was charged separately with PA (222.15 mg, 1.5 mmol, 100 equiv.) and CHO (725.15 mg, 7.5 mmol, 500 equiv.), then three freeze-thaw cycles were carried out. The cell was degassed, exposed to 365 nm irradiation (65 mW·cm^{-2}) for 5 min, then the solution was immediately added to the Schlenk tube under inert atmosphere. The polymerization was conducted at 110°C for 1 h and PA monomer conversion was monitored by ^{1}H-NMR in $CDCl_3$. After reaction time, the crude sample was diluted in $CHCl_3$ and precipitated in methanol. The polymer was filtered under vacuum and dried under vacuum at 60 °C until a constant weight was achieved. The resultant polymer was then analyzed by SEC.

2.4 Synthesis of polynorbornene. NB (0.047 g, 5 × 10^{-4} mmol, 510 equiv.), **1H$^+$BPh$_4^-$** (3 mg, 4.90 × 10^{-3} mmol, 5 equiv.), ITX (0.63 mg, 2.48 × 10^{-3} mmol, 2.5 equiv.) and $[RuCl_2(p\text{-cymene})]_2$ (0.60 mg, 9.8 × 10^{-4} mmol, 1 equiv.) and CD_2Cl_2 (1 M relative to NB, 0.5 ml) were placed in a 5 mL vial. The solution was mixed, transferred to a borosilicate NMR tube. The polymerization was conducted inside a LED circular photochemical reactor at room temperature. The photoreactor was constructed by winding a 365 nm LED strip (SMD3528, 60 LED/Meter, Lightingwill, length: 1000 mm) around a quartz cylinder (internal diameter: 60 mm, length: 200 mm). The NMR tube was introduced in the axis of the quartz cylinder where it received an irradiance of 6.5 mW·cm^{-2}. All samples were irradiated for 60 s. Monomer conversion and *cis*/*trans* ratio were monitored by ^{1}H-NMR analysis. Reactions were quenched by adding an excess amount of vinyl ethyl ether, the resultant polymer was precipitated in acetone. The collected polynorbornene was washed several times with acetone and air dried for 48 h before SEC analysis.

3. Characterization methods

3.1 ^{1}H NMR analysis of NHC-carbodiimide adduct. Four similar borosilicate NMR tubes containing **1H$^+$BPh$_4^-$** (9.18 mg, 0.015 mmol, 3 equiv.), ITX (3.82 mg, 0.015 mmol, 1 equiv.) and THF-d_8 (0.03 M, relative to **1H$^+$BPh$_4^-$**, 0.5 mL) were degassed with N_2. Subsequently, each tube was exposed to the UV irradiation of a 365 nm LED (LC-L1V3, Hamamatsu, 65 mW·cm^{-2}) for a given time: 1 min, 2 min, 5 min and 10 min (when CQ was used instead of ITX, a 450 nm LED was employed: MP-LE1007, Metaphase, 55 mW·cm^{-2}). Prior to the addition of CDI (3.35 mg, 0.015 mmol, 3 equiv.), deprotonation of **1H$^+$BPh$_4^-$** was monitored by ^{1}H-NMR. After CDI introduction, a change of color of the reaction medium took place from yellow/brown to pale/ dark orange. The solution was left for 2 min, then a ^{1}H-NMR spectrum was recorded. All yields were calculated following equation (1) below:

$$\text{Yield (\%)} = \frac{3(I_{6.26-6.28} + I_{5.76-5.78})}{3(I_{6.26-6.28} + I_{5.76-5.78}) + 4(I_{2.37})} \times 100 \qquad (1)$$

where $I_{6.26\text{-}6.28}$, $I_{5.76\text{-}5.78}$ are the intensity of methine protons ($\delta_{m'}$= 6.26 – 6.28 ppm, $\delta_{n'}$= 5.76 – 5.78 ppm) of **1**-CDI adduct and $I_{2.37}$ is the intensity of methyl proton in *para* position (δ = 2.37 ppm) of residual **1H$^+$BPh$_4^-$**.

3.2 Electron spin resonance (ESR) of NHC-radical adduct. **1H$^+$BPh$_4^-$** (9.18 mg, 0.015 mmol, 3 equiv.), ITX (1.27 mg, 0.005 mmol, 1 equiv.), TPO (10.4 mg, 0.033 mmol, 6 equiv.) were added to 1 mL of THF. The mixture was prepared in a small vial capped with a rubber septum. The solution was degassed with N_2, then 0.2 mL were transferred into a quartz ESR tube with an internal diameter of 2.5 mm, the solution was degassed with N_2. Subsequently, the ESR tube was irradiated with a 365 nm LED (LC-L1V3, Hamamatsu, 65 mW·cm^{-2}). ESR spectra were recorded before irradiation, and after 2 and 5 min irradiation. For the control experiment, an identical procedure was followed using the mixture of **1** (4.56 mg, 0.015 mmol, 3 equiv.) and TPO (1.04 mg, 0.003 mmol, 0.6 equiv.) in THF, cautiously prepared in a gloves box.

3.3 Steady-state photolysis. A stock solution containing ITX (1.27 mg, 0.005 mmol) was prepared in acetonitrile (2 × 10^{-4} M, 25 mL). A **1H$^+$BPh$_4^-$**/ITX solution was prepared by adding 1.10 mg of **1H$^+$BPh$_4^-$** (0.0018 mmol) into a conventional spectroscopic cell containing 3 mL of the ITX solution and a micro magnet bar. The cell was capped with a rubber septum and degassed with N_2 for 10 min before exposure to a Hg-Xe lamp (LC-9588/01A, Hamamatsu) including a filter providing a monochromatic incident irradiation (365 nm, 75 mW·cm^{-2}). Continuous stirring was maintained during irradiation. Temporal change in absorbance at 365 nm was monitored by utilizing a spectrometer (USB4000 from Ocean Optics). Other solutions in the presence or the absence of other quenchers: **2H$^+$BPh$_4^-$** (1.10 mg, 1.8 mmol), **1H$^+$Cl$^-$** (0.61 mg, 0.0018 mmol), $NaBPh_4$ (0.62 mg, 0.0018 mmol), **1** (0.55 mg, 0.0018 mmol) and **2** (0.554 mg, 0.0018 mmol) were also conducted following the aforementioned procedure.

3.4 Cyclic voltammetry measurement and calculation of free energy for electron-transfer. Four different solutions with a similar concentration (4×10^{-2} M) were prepared from $\mathbf{1H^+Cl^-}$, $NaBPh_4$, $\mathbf{2H^+BPh_4^-}$ and $\mathbf{1H^+BPh_4^-}$. Cyclic voltammetry measurement was conducted as previously described.[36] Based on the cyclic voltammetry plots, oxidation potentials at 0.83, 0.96 and 0.94 eV (*vs.* saturated calomel electrode (SCE)) were measured, and respectively assigned to oxidation of BPh_4^- ($NaBPh_4$), BPh_4^- ($\mathbf{2H^+BPh_4^-}$) and BPh_4^- ($\mathbf{1H^+BPh_4^-}$). No oxidation potential was detected in case of $\mathbf{1H^+Cl^-}$. After a first cycle, new intense oxidation peaks at –1.52 ($\mathbf{2H^+BPh_4^-}$) and –0.84 eV vs. SCE ($\mathbf{1H^+BPh_4^-}$) became visible. Their appearance reflects the oxidation of **1** and **2** formed by electrochemical reduction of $\mathbf{2H^+}$ and $\mathbf{1H^+}$. The free energy change of photoinduced electron-transfer was estimated through the Rehm-Weller equation (2):[64]

$$\triangle G_{et} = E_{ox}(D) - E_{red}(A) - E_T + C \qquad (2)$$

where $\triangle G_{et}$ is the free energy change of photoinduced electron-transfer (PET); $E_{ox}(D)$, the oxidation potential of the electron donor; $E_{red}(A)$, the reduction potential of the electron acceptor; E_T, the triplet state energy level of electron acceptor; and C, the Coulombic stabilization energy (–0.06 V in acetonitrile).[65] Details on calculation are provided in SI.

3.5 NMR spectroscopy. All NMR spectra were recorded in appropriate deuterated solvents with tetramethylsilane (TMS) as the internal reference on a Varian 300 – MR. All chemical shifts are reported in parts per million (ppm) relative to the residual CD_2Cl_2 (δ 5.32 ppm), THF-d_8 (δ 1.72 ppm and 3.58 ppm), $CDCl_3$ (δ 7.26 ppm), DMSO-d_6S (δ 2.50 ppm) or CD_3CN (δ 1.94 ppm). Peaks multiplicities in ^{1}H – NMR spectra are abbreviated as s (single), d (double), t (triplet), m (multiplet), br (broad).

3.6 UV-Vis absorption. Absorption spectra were recorded on a Lambda 35 UV/vis spectrometer from PerkinElmer with a bandwidth of 1 nm and a scan speed of 400 nm min^{-1}. All the solutions were analyzed in a quartz cuvette of 1 cm length.

3.7 Size exclusion chromatography (SEC). An Agilent 1260 Infinity series equipped with Polymer Laboratories ResiPore columns, a G1314B wavelength detector, a MDS refractive index detector and a MDS viscosimeter detector was employed to determine the molar mass values and distributions of polyurethane and polyester samples. Precise concentration solutions of polymer in THF were prepared and injected with flow rate of 1 mL·min^{-1}. A set of EasiVial polystyrene PS-M standards was used to establish the universal calibration. High molecular weights of polynorbornene samples were determined using a SEC instrument from a Varian apparatus equipped with TOSOHAAS TSK gel columns and a refractive index detector. The mobile phase was THF at a flow rate of 1 mL·min^{-1}; the injected volume was 100 µL. The MALS instrument was normalized using a THF solution of polystyrene standard.

3.8 Electron spin resonance. ESR measurements were performed in a Brucker Elexsys E500 spectrometer with X band frequency in continuous wave (around 9.8 GHz) at room temperature. Spectra were recorded with a modulation amplitude of 1 G, a modulation frequency of 100 kHz and a microwave power of ~ 2 mW. Both Bruker WIN-ESR and SimFonia software were used for spectra treatment and simulation.

Acknowledgements

Financial support by French National Research Agency (ANR program: DS0304 2016, contract number: ANR-16-CE07-0016) is gratefully acknowledged. A.C. acknowledges the sustained support of Dr. Olivier Soppera, Dr. Julien Poly for equipment loans and Mrs. Bernadette Graff (IS2M, University of Haute-Alsace) for DFT calculations.

Keywords: N-heterocyclic carbene • latent • metathesis • photochemistry • polymerization

[1] A. J. Arduengo, R. L. Harlow, M. Kline, *J. Am. Chem. Soc.* **1991**, *113*, 361–363.
[2] B. Hogan, M. Albrecht, in *Ref. Module Chem. Mol. Sci. Chem. Eng.*, Elsevier, **2016**, p. 1–14.
[3] E. Peris, *Chem. Rev.* **2018**, *118*, 9988–10031.
[4] D. M. Flanigan, F. Romanov-Michailidis, N. A. White, T. Rovis, *Chem. Rev.* **2015**, *115*, 9307–9387.
[5] S. Naumann, A. P. Dove, *Polym. Int.* **2016**, *65*, 16–27.
[6] N. D. Clement, L. Routaboul, A. Grotevendt, R. Jackstell, M. Beller, *Chem. - Eur. J.* **2008**, *14*, 7408–7420.
[7] F. E. Hahn, M. C. Jahnke, *Angew. Chem. Int. Ed.* **2008**, *47*, 3122–3172.
[8] S. Díez-González, N. Marion, S. P. Nolan, *Chem. Rev.* **2009**, *109*, 3612–3676.
[9] M. Scholl, S. Ding, C. W. Lee, R. H. Grubbs, *Org. Lett.* **1999**, *1*, 953–956.
[10] M. Fèvre, J. Pinaud, Y. Gnanou, J. Vignolle, D. Taton, *Chem. Soc. Rev.* **2013**, *42*, 2142–2172.
[11] S. Naumann, A. P. Dove, *Polym. Chem.* **2015**, *6*, 3185–3200.
[12] N. E. Kamber, W. Jeong, S. Gonzalez, J. L. Hedrick, R. M. Waymouth, *Macromolecules* **2009**, *42*, 1634–1639.
[13] S. Naumann, S. Epple, C. Bonten, M. R. Buchmeiser, *ACS Macro Lett.* **2013**, *2*, 609–612.
[14] J. Raynaud, W. N. Ottou, Y. Gnanou, D. Taton, *Chem. Commun.* **2010**, *46*, 3203–3205.
[15] J. Pinaud, K. Vijayakrishna, D. Taton, Y. Gnanou, *Macromolecules* **2009**, *42*, 4932–4936.
[16] O. Coutelier, M. El Ezzi, M. Destarac, F. Bonnette, T. Kato, A. Baceiredo, G. Sivasankarapillai, Y. Gnanou, D. Taton, *Polym. Chem.* **2012**, *3*, 605–608.
[17] D. C. Graham, K. J. Cavell, B. F. Yates, *J. Phys. Org. Chem.* **2005**, *18*, 298–309.
[18] A. Poater, F. Ragone, S. Giudice, C. Costabile, R. Dorta, S. P. Nolan, L. Cavallo, *Organometallics* **2008**, *27*, 2679–2681.
[19] P. de Frémont, N. Marion, S. P. Nolan, *Coord. Chem. Rev.* **2009**, *253*, 862–892.
[20] H.-J. Schönherr, H.-W. Wanzlick, *Justus Liebigs Ann. Chem.* **1970**, *731*, 176–179.
[21] W. A. Herrmann, M. Elison, J. Fischer, C. Köcher, G. R. J. Artus, *Chem. - Eur. J.* **1996**, *2*, 772–780.
[22] S. Naumann, M. R. Buchmeiser, *Catal.Sci.Technol.* **2014**, *4*, 2466–2479.
[23] F. Bonnette, T. Kato, M. Destarac, G. Mignani, F. P. Cossío, A. Baceiredo, *Angew. Chem. Int. Ed.* **2007**, *46*, 8632–8635.
[24] B. Bantu, G. M. Pawar, U. Decker, K. Wurst, A. M. Schmidt, M. R. Buchmeiser, *Chem. - Eur. J.* **2009**, *15*, 3103–3109.
[25] B. C. Norris, D. G. Sheppard, G. Henkelman, C. W. Bielawski, *J. Org. Chem.* **2011**, *76*, 301–304.
[26] S. Naumann, F. G. Schmidt, W. Frey, M. R. Buchmeiser, *Polym. Chem.* **2013**, *4*, 4172–4181.
[27] N. Corrigan, J. Yeow, P. Judzewitsch, J. Xu, C. Boyer, *Angew. Chem. Int. Ed.* **2019**, *58*, 5170–5189.
[28] C. Fu, J. Xu, C. Boyer, *Chem. Commun.* **2016**, *52*, 7126–7129.
[29] D. M. Denning, M. D. Thum, D. E. Falvey, *Org. Lett.* **2015**, *17*, 4152–4155.
[30] K. Suyama, M. Shirai, *Prog. Polym. Sci.* **2009**, *34*, 194–209.

[31] E. Placet, J. Pinaud, O. Gimello, P. Lacroix-Desmazes, *ACS Macro Lett.* **2018**, *7*, 688–692.

[32] X. Dong, P. Hu, G. Zhu, Z. Li, R. Liu, X. Liu, *RSC Adv.* **2015**, *5*, 53342–53348.

[33] X. Sun, J. P. Gao, Z. Y. Wang, *J. Am. Chem. Soc.* **2008**, *130*, 8130–8131.

[34] S. Chatani, T. Gong, B. A. Earle, M. Podgórski, C. N. Bowman, *ACS Macro Lett.* **2014**, *3*, 315–318.

[35] J. Shin, H. Matsushima, C. M. Comer, C. N. Bowman, C. E. Hoyle, *Chem. Mater.* **2010**, *22*, 2616–2625.

[36] J. Pinaud, T. K. H. Trinh, D. Sauvanier, E. Placet, S. Songsee, P. Lacroix-Desmazes, J.-M. Becht, B. Tarablsi, J. Lalevée, L. Pichavant, et al., *Chem. - Eur. J.* **2018**, *24*, 337–341.

[37] S. Dadashi-Silab, C. Aydogan, Y. Yagci, *Polym. Chem.* **2015**, *6*, 6595–6615.

[38] A. M. Sarker, A. Lungu, A. Mejiritski, Y. Kaneko, D. C. Neckers, *J. Chem. Soc. Perkin Trans. 2* **1998**, 2315–2322.

[39] S. Chatterjee, P. D. Davis, P. Gottschalk, M. E. Kurz, B. Sauerwein, X. Yang, G. B. Schuster, *J. Am. Chem. Soc.* **1990**, *112*, 6329–6338.

[40] B. Tumanskii, D. Sheberla, G. Molev, Y. Apeloig, *Angew. Chem.* **2007**, *119*, 7552–7555.

[41] D. Sheberla, B. Tumanskii, A. C. Tomasik, A. Mitra, N. J. Hill, R. West, Y. Apeloig, *Chem. Sci.* **2010**, *1*, 234–241.

[42] A. Baishya, L. Kumar, M. Kr. Barman, T. Peddarao, S. Nembenna, *ChemistrySelect* **2016**, *1*, 498–503.

[43] A. V. Zhukhovitskiy, J. Geng, J. A. Johnson, *Chem. - Eur. J.* **2015**, *21*, 5685–5688.

[44] O. Hollóczki, *Phys. Chem. Chem. Phys.* **2016**, *18*, 126–140.

[45] M. Feroci, I. Chiarotto, F. D'Anna, F. Gala, R. Noto, L. Ornano, G. Zollo, A. Inesi, *ChemElectroChem* **2016**, *3*, 1133–1141.

[46] M. Thomas, M. Brehm, O. Hollóczki, B. Kirchner, *Chem. - Eur. J.* **2014**, *20*, 1622–1629.

[47] N. S. Allen, F. Catalina, J. Luc-Gardette, W. A. Green, P. N. Green, W. Chen, K. O. Fatinikun, *Eur. Polym. J.* **1988**, *24*, 435–440.

[48] T. Konishi, Y. Sasaki, M. Fujitsuka, Y. Toba, H. Moriyama, O. Ito, *J. Chem. Soc. Perkin Trans. 2* **1999**, 551–556.

[49] T. Ramnial, I. McKenzie, B. Gorodetsky, E. M. W. Tsang, J. A. C. Clyburne, *Chem. Commun.* **2004**, *0*, 1054–1055.

[50] Y. Toba, M. Sakamoto, T. Uesugi, *J. Photopolym. Sci. Technol.* **1999**, *12*, 115–120.

[51] I. Pyszka, Z. Kucybala, J. Paczkowski, *Macromol. Chem. Phys.* **2004**, *205*, 2371–2375.

[52] H. Sardon, A. Pascual, D. Mecerreyes, D. Taton, H. Cramail, J. L. Hedrick, *Macromolecules* **2015**, *48*, 3153–3165.

[53] S. Paul, Y. Zhu, C. Romain, R. Brooks, P. K. Saini, C. K. Williams, *Chem. Commun.* **2015**, *51*, 6459–6479.

[54] E. Hosseini Nejad, C. G. W. van Melis, T. J. Vermeer, C. E. Koning, R. Duchateau, *Macromolecules* **2012**, *45*, 1770–1776.

[55] S. Naumann, M. Speiser, R. Schowner, E. Giebel, M. R. Buchmeiser, *Macromolecules* **2014**, *47*, 4548–4556.

[56] H. J. Altmann, S. Naumann, M. R. Buchmeiser, *Eur. Polym. J.* **2017**, *95*, 766–774.

[57] A. C. Hillier, W. J. Sommer, B. S. Yong, J. L. Petersen, L. Cavallo, S. P. Nolan, *Organometallics* **2003**, *22*, 4322–4326.

[58] J. Huang, H.-J. Schanz, E. D. Stevens, S. P. Nolan, *Organometallics* **1999**, *18*, 2370–2375.

[59] A. Tudose, A. Demonceau, L. Delaude, *J. Organomet. Chem.* **2006**, *691*, 5356–5365.

[60] L. Delaude, M. Szypa, A. Demonceau, A. F. Noels, *Adv. Synth. Catal.* **2002**, *344*, 749–756.

[61] L. Delaude, A. Demonceau, A. F. Noels, *Curr. Org. Chem.* **2006**, *10*, 203–215.

[62] X. Bantreil, S. P. Nolan, *Nat. Protoc.* **2011**, *6*, 69–77.

[63] Y. Zhang, D. Wang, P. Lönnecke, T. Scherzer, M. R. Buchmeiser, *Macromol. Symp.* **2006**, *236*, 30–37.

[64] D. Rehm, A. Weller, *Isr. J. Chem.* **1970**, *8*, 259–271.

[65] N. J. Turro, J. C. Scaiano, V. Ramamurthy, *Modern Molecular Photochemistry of Organic Molecules*, University Science Books, Sausalito, Calif, **2010**, p.383–483.

Entry for the Table of Contents

FULL PAPER

Text for Table of Contents

25 years after Arduengo's report, NHCs still require inert atmosphere and harsh conditions for their generation. To overcome this issue, the first air-stable NHC photogenerator has been developed which simplifies storage and handling. Our multidisciplinary study covers photochemical mechanism, new means to identify and quantify photogenerated NHCs, and the development of three different NHC-mediated photopolymerizations.

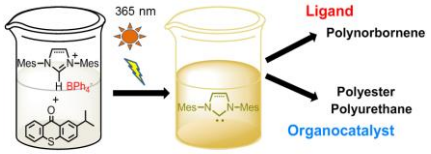

Thi Kim Hoang Trinh Jean-Pierre Malval, Fabrice Morlet-Savary, Julien Pinaud[l] Patrick Lacroix-Desmazes, Corine Reibel, Valérie Héroguez, and Abraham Chemtob

Page No. – Page No.

Mixture of Azolium Tetraphenylborate with Isopropylthioxanthone: a New Class of N-Heterocyclic Carbene (NHC) photogenerator for Polyurethane, Polyester and ROMP Polymers Synthesis